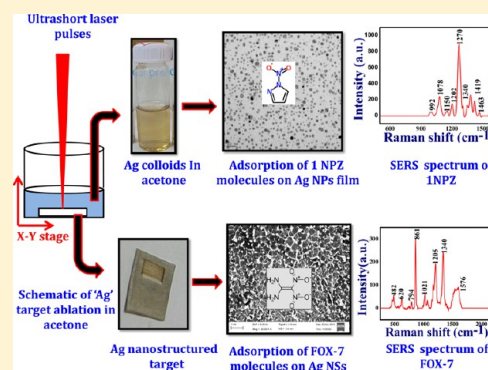


Trace-Level Detection of Secondary Explosives Using Hybrid Silver–Gold Nanoparticles and Nanostructures Achieved with Femtosecond Laser Ablation

G. Krishna Podagatlapalli,[†] Syed Hamad,[‡] and S. Venugopal Rao^{*,†}[†]Advanced Center of Research in High Energy Materials (ACRHEM) and [‡]School of Physics, University of Hyderabad, Prof. C. R. Rao Road, Hyderabad 500046, Telangana, India

S Supporting Information

ABSTRACT: Hybrid silver–gold targets were achieved by effortless mixing of pure silver (Ag) and gold (Au) metals at different ratios ($\text{Ag}_{0.65}\text{Au}_{0.35}$, $\text{Ag}_{0.5}\text{Au}_{0.5}$, and $\text{Ag}_{0.35}\text{Au}_{0.65}$) and embracing a manual melting process. The obtained targets were ablated by ultrafast (~ 40 fs) laser pulses in acetone ensuing the fabrication of Ag–Au bimetallic nanoparticles (NPs) and nanostructures (NSs) in a single experiment. UV–visible extinction spectra of Ag–Au colloids demonstrated the tuning of localized surface plasmon resonance (LSPR) in the spectral range of 406–524 nm. The morphologies of NSs were investigated by the field emission scanning electron microscopy (FESEM) technique. Ag–Au NPs and NSs were utilized as surface enhanced Raman scattering (SERS) platforms to detect secondary explosive molecules such as 1,1-diamino-2,2-dinitroethene (FOX-7, 5 μM concentration) and 1-nitro pyrazole (INPZ, 20 nM concentration). Our experimental observations clearly demonstrated that the increment in gold percentage reduced the surface activity of Ag–Au NPs/NSs. The estimated enhancement factors (EFs) from the SERS data were typically $>10^8$. Our detailed investigations revealed that the NPs and NSs of $\text{Ag}_{0.65}\text{Au}_{0.35}$ exhibited significant EFs compared to other ratios and pure metals of Ag and Au.



INTRODUCTION

Fabrication of pure plasmonic metal (Au, Ag, and Cu) nanoparticles (NPs) achievable through sophisticated chemical methodologies is well established and understood by the scientific community. However, many of these methods demands hours of monitoring and post production processes such as cleaning the nanomaterials to remove chemical dopants and impurities. Similarly, shape controlled production of bimetallic NPs through utilizing surfactants and reagents is also well-known in chemical methods. Many of the earlier reports revealed that bimetallic (Au–Ag, Ag–Cu, and Au–Cu) NPs were fabricated by adding individual colloidal solutions of gold, silver, and copper with different proportions to achieve hybridization of the localized surface plasmon resonances (LSPRs). Ultrafast laser ablation in liquids (ULAL) is a clean, green method which does not utilize chemicals for fabrication of NPs/NSs, and importantly, it does not necessitate extreme cleaning of NPs/NSs. Moreover, simultaneous fabrication of NPs and NSs is possible in the ULAL technique^{1–15} in contrast to other chemical methods. Even though some of the solution (chemical) methods are fast (in terms of time taken) compared to various ablation techniques, the main problem with them is that the capped ligand molecules sit on surface of NPs and thus blocks the analyte molecules to achieve direct contact with NP surface. The main objective of fabricating alloy nanomaterials is to find out the exact proportion of individual metals, which exhibits superior performance (in this case, our interest is in the

surface enhanced Raman signal) and, hence, are versatile and compatible in many fields such as biomedicine, spectroscopy, and photonics. For example, it has been demonstrated that Ag–Au NPs possessed a higher ability as strong catalysts compared to their individual metal counterparts.^{17–21} In the specific case of Ag–Au NPs, individual demerits of silver (often suffers oxidation effects compared to gold) and gold (weak SPR strength compared to silver) can be circumvented through the hybridization process. As a consequence, new mechanical, thermal properties can be incorporated in hybridized nanomaterials through which one can produce both chemically stable and thriving optically responsive materials such as Ag–Au NPs/NSs. Particularly, hybridization significantly influences the SPR peak position and its bandwidth, which primarily depends upon the individual proportion of the metals in the composite. Hybridization of silver and gold leads to surface plasmon (SP) absorption tunability in the absorption bands of individual Ag and Au NPs.²² The tunability of combined resonance of Au–Ag NPs over a wide spectral range is essential in many applications in which the optical field enhancements (mediated by surface plasmons) are exploited.²¹ Due to the tunability of SPRs, these Ag–Au NPs have many applications in nonlinear optics as optical limiters.²² In addition, Au–Ag NPs have

Received: April 25, 2015

Revised: June 24, 2015

Published: June 24, 2015

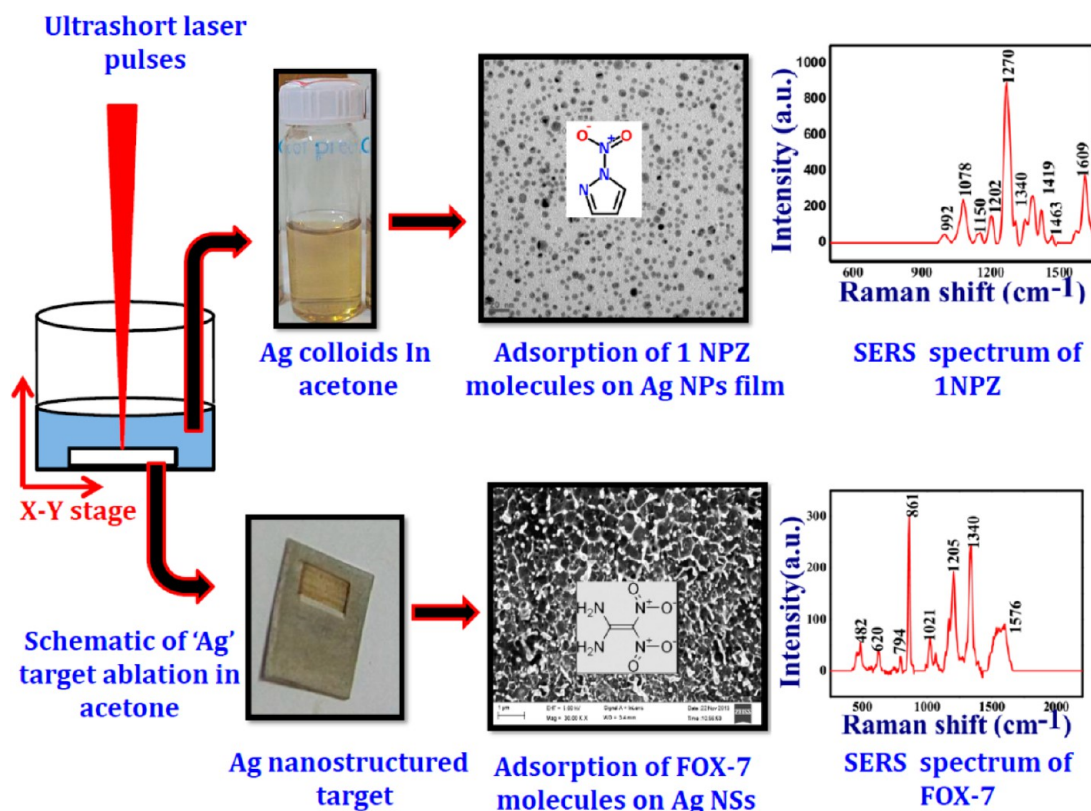


Figure 1. Complete picture of laser ablation metals in aqueous media and their utilization for surface enhanced Raman spectroscopic studies.

applications in solar cell fabrication, microelectronics, and sensor fabrication.²³ In solar cell fabrication, the efficiency of the cell can be improved by utilizing the plasmonic metallic/bimetallic NPs which scatter the light efficiently and trap optical energy through SPR.^{24,25}

Our earlier works on ULAL focused on optimizing the generation of NPs and NSs by changing the surrounding liquid,⁵ scanning parameters,⁶ input angle of incidence,⁷ the shape of input laser pulses,⁸ etc. A few of the earlier reports suggested the fabrication of Ag–Au NPs (a) based on post irradiation of colloidal mixtures by laser pulses inducing an alloying process,¹⁶ which was reported to occur through core–shell intermediates¹⁸ (b) entailing ablation of silver targets in the presence of gold nanoparticles.²¹ In the present study, Ag–Au NPs have been fabricated along with Ag–Au NSs from the alloy targets prepared prior to ablation. The prepared NPs and NSs were characterized using UV–visible absorption and field emission scanning electron microscopy (FESEM) techniques. Significantly, both the NPs and NSs were utilized as surface enhanced Raman scattering (SERS) targets for trace level detection of secondary explosive molecules such as 1,1-diamino-2,2-dinitroethene (FOX-7, 5 μ M concentration) and 1-nitro pyrazole (1NPZ, 20 nM concentration). A substantial enhancement in the Raman signals was observed for the alloy Ag_{0.65}Au_{0.35} compared to others. The advantages with nanostructured targets prepared using these techniques are that they can be prepared over a large area (few mm², easily scalable to few inch², and is only limited by the translation stages used for scanning the target placed in liquids) and are equitably reproducible. Furthermore, recent advances and detailed understanding of the ultrafast ablation phenomena enables rapid generation of NPs at grams/hour rates.¹⁴ Rapid advances in the fs laser technologies and adaptive optics enables the preparation

of these nanostructured targets in large quantities and over a short period of time (multiplexing is another possibility). Furthermore, compared to nanoparticles, nanostructures are more robust and rugged and need a lesser amount of preparation for performing SERS studies. Our earlier reports¹⁰ based on copper nanostructures revealed that these substrates can be used multiple times through adoption of an appropriate cleaning procedure, thereby enabling detection of multiple, diverse molecules using a single nanostructured substrate. To the best of our knowledge, this is the first report on utilization of both NPs (colloids) and NSs (laser fabricated targets) prepared in a single experiment for the SERS measurements of explosive molecules.

EXPERIMENTAL DETAILS

Ag–Au Metal Target Preparation. Most of the bimetallic (Ag–Au, Au–Cu, Ag–Cu) nanomaterial preparations reported so far were based on chemical methods which are usually complicated and require practice of vigorous cleaning procedures post fabrication.^{26–30} Any residual chemical moieties left on the nanomaterial surface lead to unwanted consequences. Most of the researchers prepared Ag–Au NPs by mixing individual Ag and Au colloids (at different proportions) followed by laser beam irradiation to produce bimetallic/alloy NPs.^{31–33} Some of them are a mixture of chemical and physical processes such as ablating a bulk plasmonic metal target in solutions such as HAuO₄ or AgNO₃.^{34,35} However, in the present study, we tried to prepare bulk Ag–Au targets by mixing through melting the gold and silver at different proportions (1 g of Ag + 0.5 g of Au, 0.5 g of Ag + 0.5 g of Au, 0.5 g of Ag + 1 g of Au) and were successful. The alloys were prepared by mixing the melts of Ag and Au thoroughly and subsequent to cooling the targets were immediately (within

2–3 h) used for ablation to avoid any undesirable surface effects. Prior to ablation, the Ag–Au metal targets were cleaned to remove any surface contaminants produced in the due course of melting and subsequently small strips of 1 cm × 1 cm dimensions were prepared. The cleaned Ag–Au strips were then utilized to fabricate NPs and NSs through ablation utilizing ~40 fs laser pulses in the presence of acetone. The important difference in the present ablation case (compared to other studies) is that the target was translated while ablation took place.

A detailed experimental procedure of ablation in liquid media was reported in our earlier works.^{5–9} Briefly, the Ag–Au target was immersed in HPLC grade acetone in a Pyrex cell and was placed on a motorized nanodirect XYZ stage. The thickness of the liquid layer on the target surface in the Pyrex cell was ~6 mm. Fs laser pulses were focused vertically onto the Ag–Au target through a plano-convex lens ($f = 25$ cm). The focal plane was adjusted on the target surface by observing the plasma, which appeared with a cracking sound, as the reference.^{36,37} To estimate the displacement of the focal plane in the presence of acetone, initially the focus was adjusted on the target surface in the absence of acetone. Later, depending on the thickness of the liquid layer, the amount of focal plane displacement was estimated using the relation $d = 1 \times (n - 0.5)$, which is the function of the linear refractive index (n) of the liquid medium.³⁸ In the nanodirect XYZ stage, the vertical stage (Z) was utilized to adjust the focal point on the target surface and the other two stages were utilized to draw periodic lines with a separation of ~25 μm . The length of each line was ~3 mm and speeds of X , Y stages were ~100 $\mu\text{m/s}$, ~500 $\mu\text{m/s}$, respectively. The duration of ablation for each sample was typically 40 min. Typical input energies used were ~150 μJ . The beam waist on the target surface in acetone was measured (from SEM data) to be ~50 μm . The repetition rate was 1 kHz, and the speed of the stage was ~100 $\mu\text{m/s}$. Taking these values into account, the approximate number of pulses per spot is $\omega(z)/d$, where $\omega(z)$ is the laser spot and d is the pulse-to-pulse separation distance (0.1 μm). The effective number of pulses estimated for the double line ablation case was $2 \times 50/0.1 = 1000$. Thus, the estimated fluence was ~8 J/cm^2 . After completion of ablation, the targets were removed and cleaned thoroughly. Similarly, colloidal solutions were collected in air tightened vessels and stored, preventing it from oxidation. In the present work, we have (a) fabricated bulk Ag–Au targets through combining individual Ag and Au metal melts at different proportions, (b) investigated fabrication of Ag–Au bimetallic NPs and NSs through ultrafast laser ablation in acetone, and (c) utilized the prepared Ag–Au NPs and NSs as platforms for SERS studies of explosive molecules. The evaluation of the surface activity of Ag–Au NPs and NSs was performed on the basis of Ag and Au proportions. A complete schematic of the ablation scheme and utilization of both the nanoparticles (nanocolloids in solution) and nanostructures (fs laser modified solid targets) for SERS studies is illustrated in Figure 1.

RESULTS AND DISCUSSION

XRD Characterization. After preparing the Ag–Au targets, their bimetallic phase was confirmed by X-ray diffraction (XRD) with the Cu $K\alpha$ line and the data is presented in Figure 2. Four peaks in each spectrum of Figure 2 represent the Ag–Au phase with the planes (1 1 1), (2 0 0), (2 2 0), and (3 1 1). The planes observed in the bimetallic phase of Ag–Au are

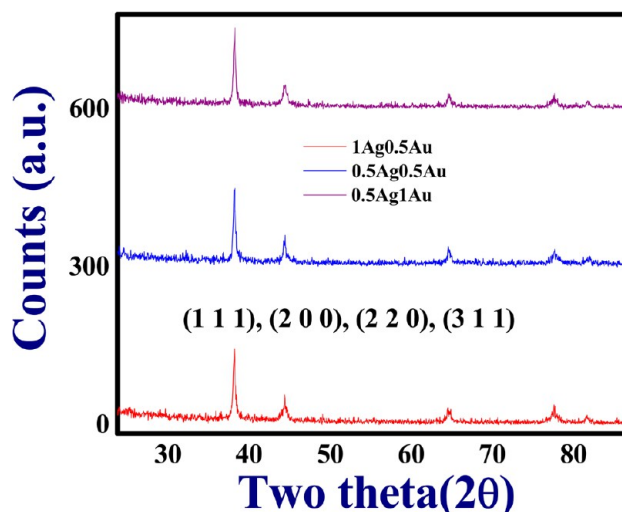


Figure 2. XRD spectra of bimetallic targets after preparation. Red, $\text{Ag}_{0.65}\text{Au}_{0.35}$; blue, $\text{Ag}_{0.5}\text{Au}_{0.5}$; violet, $\text{Ag}_{0.35}\text{Au}_{0.65}$.

similar to that of individual Ag or Au, since their lattice constants are similar [Au (0.408 nm) and Ag (0.4089 nm)].³⁹ This similarity of Ag and Au lattice constants facilitates the mixing of Ag and Au at any proportion. After the confirmation of the bimetallic phase, we proceeded to ablate Ag–Au targets in acetone. The main objective behind the fabrication of Ag–Au bimetal nanomaterials in the present study is to investigate whether mere mixing of melts leads to hybridization of localized surface plasmon resonances (LSPRs) or not. Moreover, both Ag and Au are similar metals with nearly equal lattice constants enabling their easier amalgamation compared to other combinations such as Ag–Cu and Au–Cu. Following the experiments, we confirmed that mixing of Ag and Au was an easy task compared to the other combinations, since the Ag–Au system can be considered as a model due to their extreme miscibility at all proportions.

UV–vis Absorption Data. The UV–vis absorption spectra of colloidal Au–Ag bimetallic NPs were recorded immediately after preparation using a Jasco-V-670 spectrometer equipped with an integrating sphere in the spectral range 250–1000 nm. Figure 3a depicts the normalized UV–vis absorption spectra of Ag–Au colloids of different proportions prepared in acetone. The recorded spectra demonstrated the tuning of LSP resonance in the ~406 nm (pure Ag colloids) to ~524 nm (pure Au colloids) spectral range. LSPR peak positions for different volumetric ratios of Ag and Au, namely, $\text{Ag}_{0.65}\text{Au}_{0.35}$, $\text{Ag}_{0.5}\text{Au}_{0.5}$, and $\text{Ag}_{0.35}\text{Au}_{0.65}$ colloids, were located at ~430, ~452, and ~470 nm, respectively. LSPR peak positions of pure Ag and Au NPs in acetone were at ~406 and ~524 nm, respectively. It was observed that the LSPR peak position of Ag–Au bimetallic colloids was located at an intermediate position of intrinsic Ag and Au LSPRs. The single LSPR peak in the UV–visible spectra of alloy NPs clearly suggests the absence of any core–shell type of NPs in colloidal solution.^{32,40} In contrast to ordinary Au–Ag bimetallic NPs, Au–Ag bimetallic core–shell NPs comprise two LSPR peak positions.³² Therefore, two plasmon bands are expected if the clusters comprise the individual Au and Ag NPs/Ag–Au bimetallic NPs with core–shell structure.^{22,40,41}

Figure 3a shows the normalized (with the strongest value) absorption data of the UV–vis absorption spectrum of each volumetric ratio. It is well understood that the intensity of

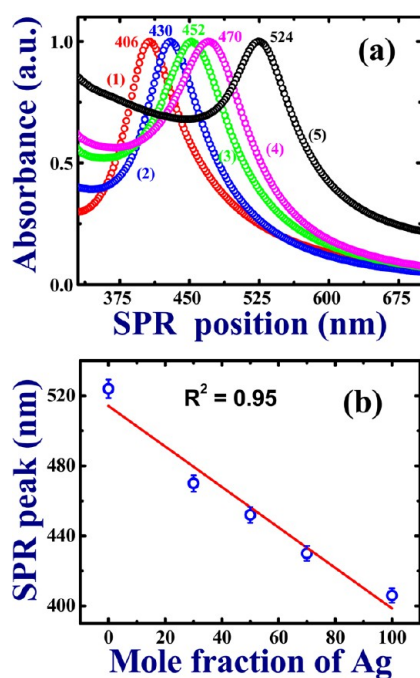


Figure 3. (a) UV-vis absorption spectra of Au-Ag colloids, namely, (1) pure Ag, (2) $\text{Ag}_{0.65}\text{Au}_{0.35}$, (3) $\text{Ag}_{0.5}\text{Au}_{0.5}$, (4) $\text{Ag}_{0.35}\text{Au}_{0.65}$, and (5) pure Au in acetone recorded after 1 day of ablation; (b) variation of LSPR peak position as a function of the mole fraction of Ag. The open circles (blue) are experimental data, while the solid line (red) is a linear fit.

spectra, LSPR peak position, and full width at half-maximum (fwhm) purely depend on the volumetric mole fraction of individual metals. The absorption spectra without normalization (shown in Figure 1 of the Supporting Information) demonstrated the differences in absorbance between the pure metal and bimetal colloids. Even at constant irradiation times

(of ~ 40 min), a different absorbance was observed in each case, confirming the ablation for diverse volumetric ratios is different. Figure 3b demonstrates the red shift of LSPR as the Ag fraction diminished in the composition. UV-visible absorption spectra demonstrated the complete amalgamation of Ag and Au atoms to produce a single hybridized LSPR peak position. Data from the UV-visible absorption spectra confirmed the formation of Ag-Au bimetallic NPs achieved by a simple, yet effective, method of mixing individual Au and Ag melts. Moreover, LSPR peak positions are weakly dependent on size and strongly dependent on the composition of the material fraction.⁴²⁻⁴⁵ We had fabricated Ag-Au NPs by ablating the bimetallic targets in a highly polar liquid, acetone. After the ablation, Ag-Au NPs ejected from the bulk target remain in the surrounding liquid media as colloids. Later, these colloids were preserved in air-tightened vessels. Hybridization of silver and gold aids in overcoming the oxidation effects of silver and weak plasmon resonances of gold. The stability of Ag-Au alloy NPs sustained for 12 weeks after ablation. The stability was examined by recording the UV-visible absorption spectra every week post ablation. Here, we refer to the stability of nanoparticles from its ability to avoid aggregation. If the colloids do not aggregate over a period of time, then we define them as stable colloids. There was no such observation in our case which was confirmed from the unchanged localized surface plasmon resonance (LSPR) position in the absorption spectra recorded at different points in time.

The molar fraction was determined from the amount of silver and gold utilized to prepare a bulk bimetallic target. If the fabricated NPs are assumed to be of core-shell type, they usually exhibit two distinct LSPR peaks in the UV-visible absorption spectra. Nevertheless, we did not observe any double peaks in the recorded spectra. We observed only single peaks in the spectra, which possibly indicate the amalgamation of Ag and Au atoms those mixed into single entity. We believe that interpenetration of silver and gold lattices could have

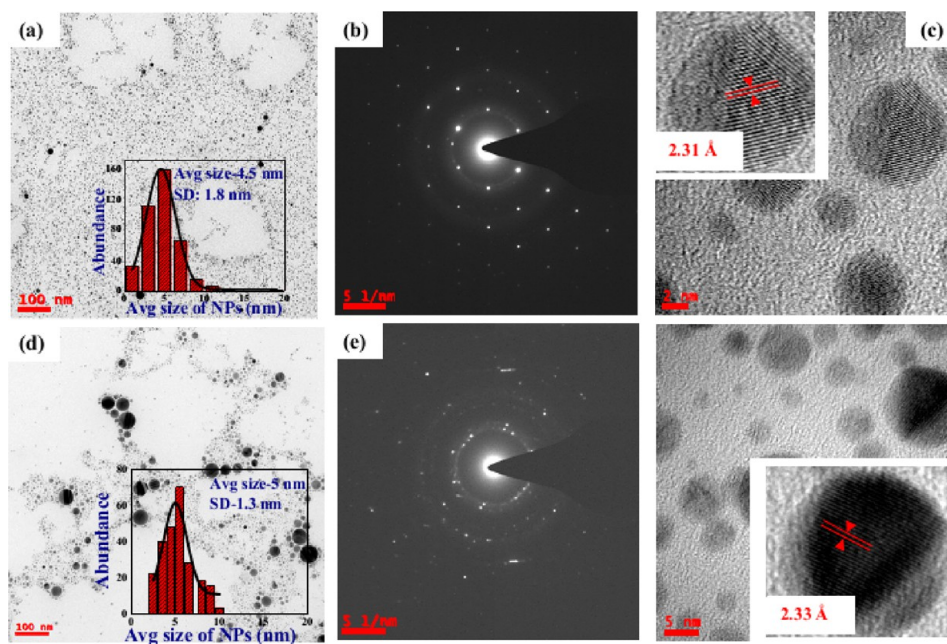


Figure 4. TEM images of (a) pure Ag NPs fabricated in acetone and their size distribution, (b) corresponding SAED pattern, and (c) HRTEM image. TEM images of (d) $\text{Ag}_{0.65}\text{Au}_{0.35}$ bimetallic NPs fabricated in acetone and their size distribution, (e) corresponding SAED pattern, and (f) HRTEM image.

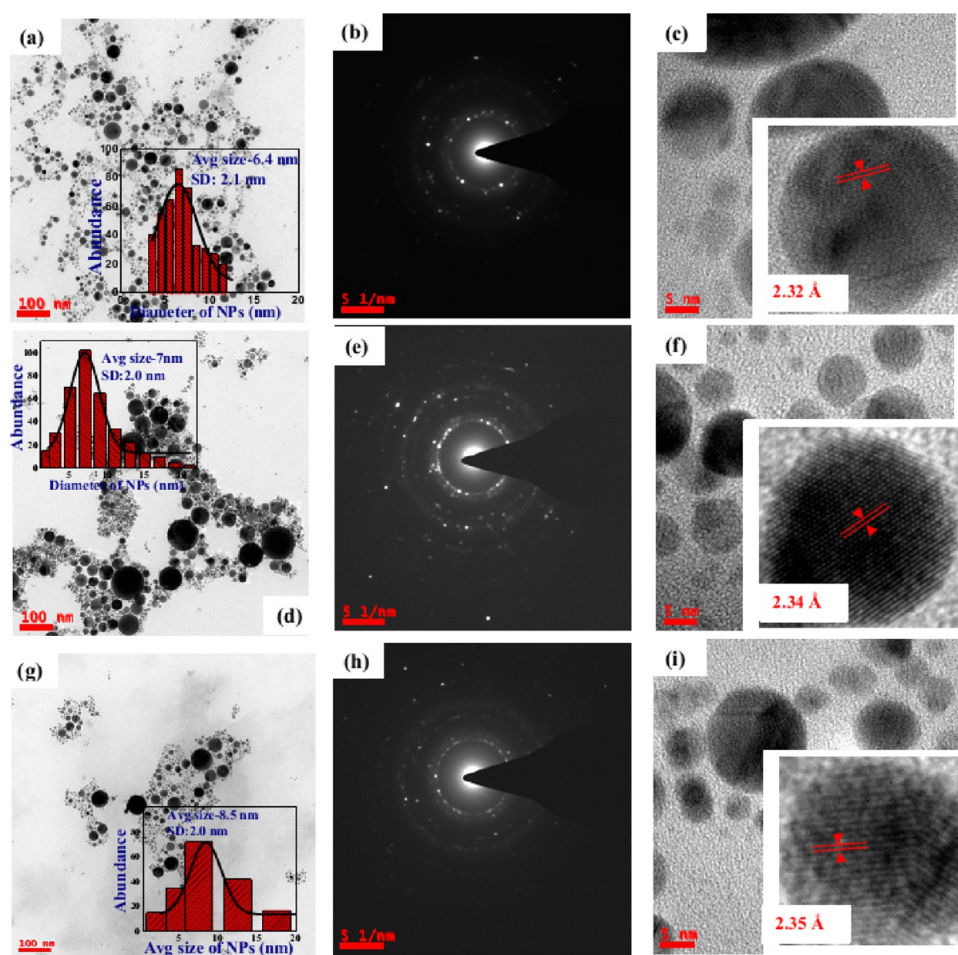


Figure 5. TEM images of (a) $\text{Ag}_{0.5}\text{Au}_{0.5}$ bimetallic NPs fabricated in acetone and their size distribution, (b) corresponding SAED pattern, and (c) HRTEM image. TEM images of (d) $\text{Ag}_{0.35}\text{Au}_{0.65}$ bimetallic NPs fabricated in acetone and their size distribution, (e) corresponding SAED pattern, and (f) HRTEM image. TEM images of (g) pure Au NPs fabricated in acetone and their size distribution, (h) corresponding SAED pattern, and (i) HRTEM image.

occurred, resulting in exhibition of such amalgamated SPRs. It is also well established that gold and silver mix thoroughly at all proportions and is a thermodynamically favorable process. A very recent report,⁴⁶ wherein nanosecond ablation was performed on the Ag/Au alloys, clearly demonstrated that the Ag and Au atoms were randomly distributed throughout the nanoparticle and no preferential sites were observed. They used the techniques of EDS in STEM mode as well as metal mapping for their studies. We would expect similar features in our studies too. Further, studies by Lee et al.⁴⁰ clearly demonstrated the stoichiometry was retained in the nanosecond ablation of Ag–Au alloys in water. However, the exact proportion of Ag and Au in a single NP and their distribution in the fs ablation case requires further detailed investigations.

TEM Analysis. Dispersions of Ag–Au NPs in acetone were characterized by transmission electron microscope (TEM, SEI cecnai G2 S-Twin200 kV) which provided an estimate of size distribution, morphologies, and crystallographic phases of the generated NPs. Ag colloids were centrifuged on carbon coated copper grids, and the solution was allowed to dry before analysis. Well monodispersed Ag, Au, and Ag–Au NPs with spherical morphologies were obtained in acetone with ~ 40 fs laser pulses. Figure 4 illustrates the TEM, selected area electron diffraction (SAED), and high resolution transmission electron microscope (HRTEM) images of Ag NPs and $\text{Ag}_{0.65}\text{Au}_{0.35}$ NPs

in acetone. Parts a and d of Figure 4 depict the TEM image of Ag NPs and $\text{Ag}_{0.65}\text{Au}_{0.35}$ NPs, and their insets show size distribution histograms constructed utilizing Image-J software. The average sizes of Ag NPs and $\text{Ag}_{0.65}\text{Au}_{0.35}$ NPs obtained were 4.5 ± 1.8 and 5 ± 1.3 nm, respectively. Though the average sizes calculated were similar, the pictures in Figure 4a and d look different and this could be attributed to (i) TEM images generally providing a localized picture rather than a global picture. Depending on how the NPs are dispensed, the obtained pictures vary. Therefore, four to five images are considered for calculating the average sizes. (ii) Further, the ablation thresholds of pure Ag, alloys, and pure Au targets are quite different. Consequently, the yield (abundance) will be different in each case. (iii) The absorption spectra (as recorded) did not demonstrate a higher yield (abundance) for pure Ag NPs. In fact, the alloy NPs demonstrated a higher absorbance signifying a higher yield (iv). The thickness of targets (five of them) used in the present study was not uniform. The pure Ag target had the highest thickness (~ 1.6 mm) followed by alloys (~ 1.5 mm) and the pure Au target (~ 1.3 mm). Therefore, when replacing the bimetallic (Ag–Au) targets post ablation of the pure Ag, Au targets, there could be slight differences in the focusing conditions, resulting in a different yield, though the experiments were performed under similar conditions of laser energy, scan speeds, etc. (v) The

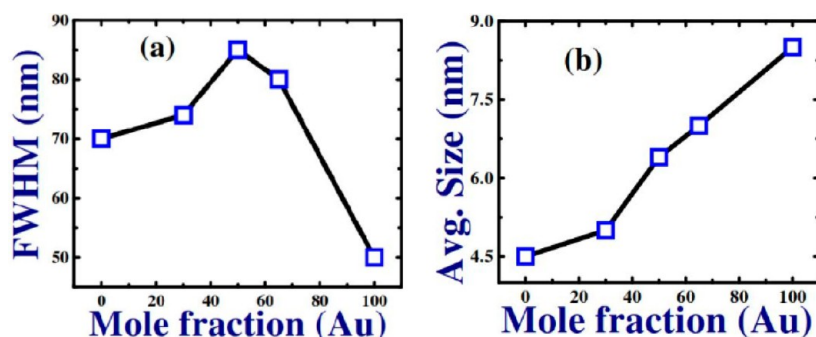


Figure 6. (a) FWHM of NPs obtained from the UV-vis extinction spectra of Ag-Au bimetallic colloids as a function of gold mole fraction. (b) Average size of Ag-Au bimetallic NPs estimated from the TEM analysis as a function of gold mole fraction.

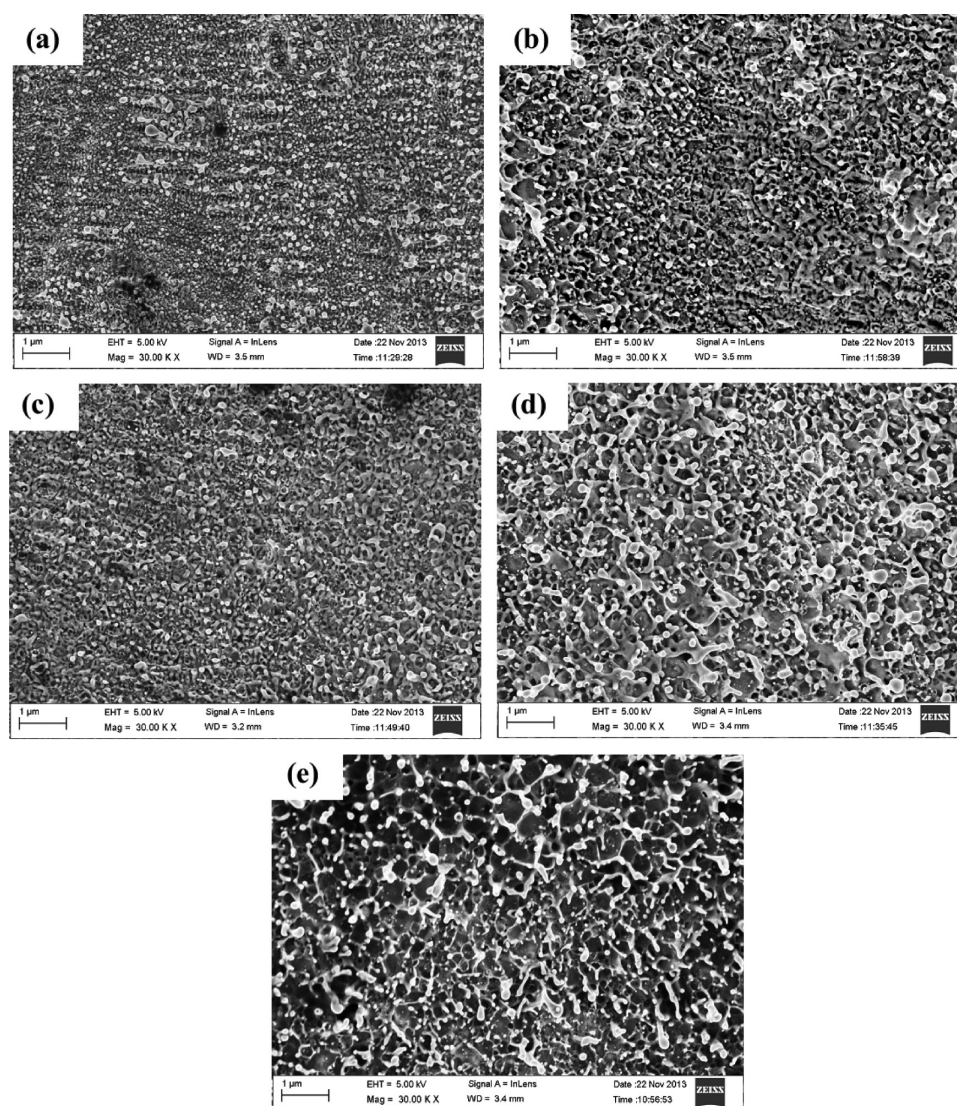


Figure 7. FESEM image of targets ablated by ~40 fs laser pulses in acetone. Laser exposed portions of the targets of (a) Ag, (b) Ag_{0.65}Au_{0.35}, (c) Ag_{0.5}Au_{0.5}, (d) Ag_{0.35}Au_{0.65}, and (e) Au.

larger sized particles were clearly present only in pure Au targets and alloy targets. Pure Ag colloids did not demonstrate such large sized NPs, indicating the ablation mechanism was different in the alloys case and the pure Au NPs case. Perhaps, the cavitation bubble dynamics played an important role in the case of alloys and pure Au ablation, resulting in different particles and yields. Parts b and e of Figure 4 represent the

SAED pattern of the fabricated Ag NPs and Ag_{0.65}Au_{0.35} NPs whose first ring diameter (~2.34 Å) gives the information of the lattice plane separations of the Miller plane (111). Measured plane separations were 2.35 and 2.26 Å for the mentioned NPs. Parts c and f of Figure 4 illustrate the HRTEM image of Ag NPs and Ag_{0.65}Au_{0.35} NPs and the measured plane separations were 2.31 and 2.33 Å.

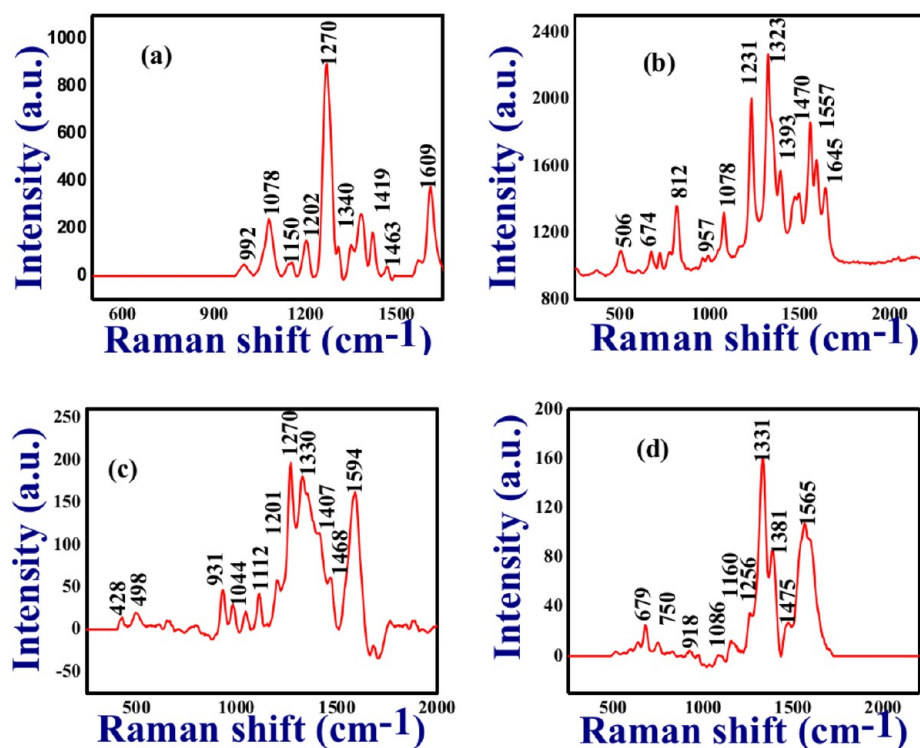


Figure 8. SERS spectra of 1NPZ (20 nM dissolved in acetone) adsorbed on (a) Ag, (b) $\text{Ag}_{0.65}\text{Au}_{0.35}$, (c) $\text{Ag}_{0.5}\text{Au}_{0.5}$, and (d) $\text{Ag}_{0.35}\text{Au}_{0.65}$ NPs drop casted on a glass slide. The time of integration was ~ 0.5 s.

Figure 5 demonstrates TEM, SAED, and HRTEM images of $\text{Ag}_{0.5}\text{Au}_{0.5}$ NPs, $\text{Ag}_{0.35}\text{Au}_{0.65}$ NPs, and Au NPs in acetone. Parts a, d, and g of Figure 5 depict the TEM images of $\text{Ag}_{0.5}\text{Au}_{0.5}$ NPs, $\text{Ag}_{0.35}\text{Au}_{0.65}$ NPs, and Au NPs, and their insets show size distribution histograms. The average size of $\text{Ag}_{0.5}\text{Au}_{0.5}$ NPs, $\text{Ag}_{0.65}\text{Au}_{0.35}$ NPs, and Au NPs obtained were 6.4 ± 2.1 , 7 ± 2 , and 8.5 ± 2 nm, respectively. While constructing the histograms of size distribution, NPs with sizes >20 nm were not considered, since their density was low compared to smaller sized NPs. Ag–Au NPs fabricated in the present set of experiments are of smaller dimensions compared to the earlier reports, which demonstrated the fabrication of Ag–Au NPs by laser ablation in liquids.⁴⁶ Parts b, e, and h of Figure 5 represent SAED patterns of the fabricated $\text{Ag}_{0.5}\text{Au}_{0.5}$ NPs, $\text{Ag}_{0.65}\text{Au}_{0.35}$ NPs, and Au NPs whose first ring diameter provides the information on the lattice plane separations of the Miller plane (111). The measured plane separations were 2.26, 2.23, and 2.27 Å for $\text{Ag}_{0.5}\text{Au}_{0.5}$ NPs, $\text{Ag}_{0.65}\text{Au}_{0.35}$ NPs, and Au NPs, respectively. Parts c, f, and i of Figure 5 illustrate the HRTEM images of $\text{Ag}_{0.5}\text{Au}_{0.5}$ NPs, $\text{Ag}_{0.65}\text{Au}_{0.35}$ NPs, and Au NPs, and the measured plane separations were 2.32, 2.34, and 2.35 Å, respectively. Lattice plane separations obtained through HRTEM images clearly indicate the miscible nature of Ag and Au metals at all proportions. This was evident from the measured lattice plane separations which were more or less equal to lattice constants of 2.36 and 2.35 Å for Ag and Au, respectively. The change in the unit cell size of Ag–Au alloy is typically less than 1% for all fractions of Ag and Au with respect to pure Ag and Au. Additionally, no super lattice reflections were observed in the prepared alloys.⁴⁷

Parts a and b of Figure 6 illustrate the FWHM from UV–visible spectra of Ag–Au bimetallic NPs and the average size of NPs from TEM images as a function of Au mole fraction. As evident from the data presented in Figure 6a, the FWHM was

observed to be highest for the combination of $\text{Ag}_{0.5}\text{Au}_{0.5}$ compared to the pure Ag or Au metal NPs. Similarly, the average size of Ag–Au NPs (Figure 6b) was highest for the fraction $\text{Ag}_{0.5}\text{Au}_{0.5}$. The FWHM of absorption/reflection spectra of Au–Ag NPs is an important parameter which enhances the efficiency of plasmonic solar cells^{48,24} and traps light inside. An important feature of these Ag–Au bimetallic NPs, compared to pure Ag or Au NPs, is that they are more suitable for fabrication of efficient plasmonic solar cells, since the bandwidth and scattering efficiency can be tuned in the entire intense solar spectrum. The data presented in Figure 6b revealed the differences in average particle size could, probably, be due to the variation of the ablation threshold of Ag–Au metals at different proportions.

FESEM Analysis. Morphologies of the laser exposed portions of Ag–Au bimetallic targets along with pure Au and Ag ablated targets were characterized by field emission scanning electron microscope [FESEM (Ultra 55 from Carl ZEISS)]. The fs laser ablated portions of the metal targets were characterized after a nominal cleaning and sonication in acetone. Figure 7 illustrates the FESEM images of laser exposed portions of Ag–Au bimetal targets along with ablated portions of pure Au and Ag targets. Specifically, Figure 7 depicts the NSs formed on (a) Ag, (b) $\text{Ag}_{0.65}\text{Au}_{0.35}$, (c) $\text{Ag}_{0.5}\text{Au}_{0.5}$, (d) $\text{Ag}_{0.35}\text{Au}_{0.65}$, and (e) Au targets, respectively. Surface morphologies of Ag, Au, and Ag–Au nanostructured targets at higher resolution are shown in Figure 2 of the Supporting Information. From the data presented in the images of Figure 7, it is apparent that the laser exposed portions of the mentioned five targets comprise grains of NPs and random grating structures which are capable of providing higher local fields when illuminated by laser beam at a suitable wavelength (through the propagating surface plasmons). The grating kind of structures play a significant role in SERS studies. As the

fraction of Au increased, the randomness of the surface morphology of laser exposed Ag–Au bimetal targets also increased. All five substrates exhibited the presence of nanostructures as well as NP grains.

SERS Studies of Au–Ag Nanoparticles and Nanostructures. The performance of fabricated Ag–Au bimetallic NPs and NSs was evaluated by recording the Raman spectra of explosive molecules such as 1NPZ (1 Nitro-Pyrazole) and FOX-7, which is a well-known derivative of DADNE, i.e., 1,1-diamino-2,2-dinitroethene. The Raman spectra of 1NPZ were recorded at 20 nM concentration from Ag–Au NPs (in film form), and the FOX-7 was recorded at 5 μ M from Ag–Au NSs. Initially, five films of Ag–Au NPs along with pure Ag and Au NPs were grown by a simple method, wherein colloidal solution of quantity 10 μ L was dropped on individual glass slides. These films were dried for some time, and later, a drop of (5 μ L) analyte solution was placed on the film to form a monolayer. After evaporation of solvent in the analyte, a glass slide was placed underneath an objective lens (100 \times) of a micro-Raman (WiTec ALPHA 300 instrument) spectrometer. The micro-Raman spectrometer utilized a continuous wave (cw) Nd:YAG laser at 532 nm. The Raman spectrometer was calibrated by recording the Raman peak of a silicon wafer at 520 cm^{-1} . In the micro-Raman spectrometer, the laser beam was focused onto the analyte molecules (adsorbed on the film of Ag–Au NPs) using a high numerical aperture objective lens (100 \times) and the estimated theoretical beam waist was \sim 700 nm. Raman signals were collected in back scattering geometry. The acquisition time used for recording spectra was 0.5 s for each trial. Figure 8 shows the SERS spectra of 1NPZ (20 nM dissolved in acetone) adsorbed on (a) Ag, (b) $\text{Ag}_{0.65}\text{Au}_{0.35}$, (c) $\text{Ag}_{0.5}\text{Au}_{0.5}$, and (d) $\text{Ag}_{0.35}\text{Au}_{0.65}$ NPs drop casted on a glass slide. It was observed that Raman signature elevation from the film of $\text{Ag}_{0.65}\text{Au}_{0.35}$ was significant compared to the others. The Raman spectra of 1NPZ powder are presented in Figure 3 of the Supporting Information. It was also observed that Au NP film did not show significant modes of Raman signatures of 1NPZ (data is shown in Figure 4a of the Supporting Information).

The enhancement factors (EFs)⁴⁹ for Ag–Au films of NPs were obtained by comparing the SERS spectra with the normal Raman spectra of 1NPZ at a higher concentration recorded on a nonplasmonic (silicon) substrate (shown in Figure 4b of the Supporting Information).

$$\text{EF} = \frac{I_{\text{SERS}} N_{\text{Raman}}}{I_{\text{Raman}} N_{\text{SERS}}}$$

where

$$N_{\text{SERS}} = \eta N_{\text{A}} V C_{\text{Sol}} \frac{A_{\text{Laser}}}{A_{\text{Substrate}}}, \quad N_{\text{R}} = N_{\text{A}} V C_{\text{Sol}} \frac{A_{\text{Laser}}}{A_{\text{Substrate}}}$$

$I_{\text{SERS}}/I_{\text{R}}$ was calculated from the area under the signature peak of the particular mode of interest. N_{SERS} - number of molecules from the laser machined Ag substrate giving rise to the surface enhanced Raman signal, N_{Raman} - number of molecules giving rise to the Raman signal from the non-SERS surface, N_{A} - Avogadro number, V - total volume of the solution added onto the substrate, A_{laser} - area of the laser spot, $A_{\text{substrate}}$ - total area of the substrate, η - adsorption factor. The adsorption factor was estimated as explained in the procedure given in our earlier reports.¹⁰ The EFs of Ag–Au bimetallic films of NPs were estimated for the mode corresponding to 1320 cm^{-1} (ring deformation + NO_2 stretch), i.e., highly elevated in the SERS

spectra and less prevailed in the normal Raman spectra of 1NPZ (0.1 M) (shown in Figure 4b of the Supporting Information). The estimated enhancement factors were $\sim 4.4 \times 10^8$, $\sim 2 \times 10^9$, $\sim 1 \times 10^8$, and $\sim 2.6 \times 10^8$ from films of Ag, $\text{Ag}_{0.65}\text{Au}_{0.35}$, $\text{Ag}_{0.5}\text{Au}_{0.5}$, and $\text{Ag}_{0.35}\text{Au}_{0.65}$ NPs, respectively. Other modes of 1NPZ and their assignments⁵⁰ are presented in Table 1. The EFs of Raman signatures of 1NPZ from Ag–Au

Table 1. Observed Active Raman Modes of 1NPZ Adsorbed on Ag–Au Film of NPs Fabricated by fs Ablation in Acetone^a

S. No.	reported Raman shifts (in cm^{-1})	assignments	observed shifts from 1NPZ powder (in cm^{-1})	observed SERS shifts from bimetallic nanomaterials (in cm^{-1})
1.	303	ring deformation + NO_2 bend		
2.	438	N– NO_2 stretch	460	428
3.	593	ring deformation + NO_2 bend	570	
4.	648	ring puckering		674, 679
5.	865	ring deformation, in plane	821	
6.	1033	ring deformation	1036	1044
7.	1076	ring deformation	1062	1078, 1086
8.	1178	ring deformation	1165	1112, 1150, 1160
9.	1263	ring deformation	1266	1231, 1256, 1270
10.	1321	ring deformation + NO_2 stretch	1320	1323, 1330, 1331, 1340
11.	1482	NO_2 stretch	1480	1463, 1465, 1470, 1475
12.	1555	NO_2 stretch	1530	1557, 1565, 1594
13.	1607	NO_2 stretch	1619	1609, 1645

^aThe time of integration was 0.5 s for all measurements.

NPs films were evaluated by considering an adsorption factor of ~ 0.3 (percentage of 1NPZ molecules adsorbed on the NSs) following the procedure reported in our earlier works.¹⁰ Raman spectra of 1NPZ from gold film of NPs did not exhibit any significant signatures. The EFs were estimated by comparing the SERS spectra with Raman spectra of 1NPZ (0.1 M) from the Si target.

Similarly, the Raman activity of Ag–Au NSs was evaluated with another high explosive molecule FOX-7 (derivative of DADNE-1,1-diamino-2,2-dinitroethene) at a concentration of 5 μ M. Before recording the Raman spectra, Ag–Au NSs were properly cleaned and the analyte solution (10 μ L) was adsorbed on the laser exposed portions of the targets. The analyte solution was allowed to dry, and later, the Raman spectra (smoothened to eliminate background and for visual clarity) were recorded. Figure 9 presents the SERS spectra of FOX-7 (5 μ M dissolved in acetone) adsorbed on (a) Ag, (b) $\text{Ag}_{0.65}\text{Au}_{0.35}$, (c) $\text{Ag}_{0.5}\text{Au}_{0.5}$, and (d) $\text{Ag}_{0.35}\text{Au}_{0.65}$ nanostructured substrates obtained using fs laser ablation. The EFs were estimated for the laser exposed Ag–Au NSs via considering the mode corresponding to 860 cm^{-1} (NO + NH rocking) in the SERS spectra. The EFs were estimated to be $\sim 7 \times 10^5$, $\sim 1 \times 10^7$, $\sim 3 \times 10^5$, and $\sim 1.2 \times 10^6$, for Ag, $\text{Ag}_{0.65}\text{Au}_{0.35}$, $\text{Ag}_{0.5}\text{Au}_{0.5}$, and $\text{Ag}_{0.35}\text{Au}_{0.65}$ NSs, respectively. The EFs of elevated Raman

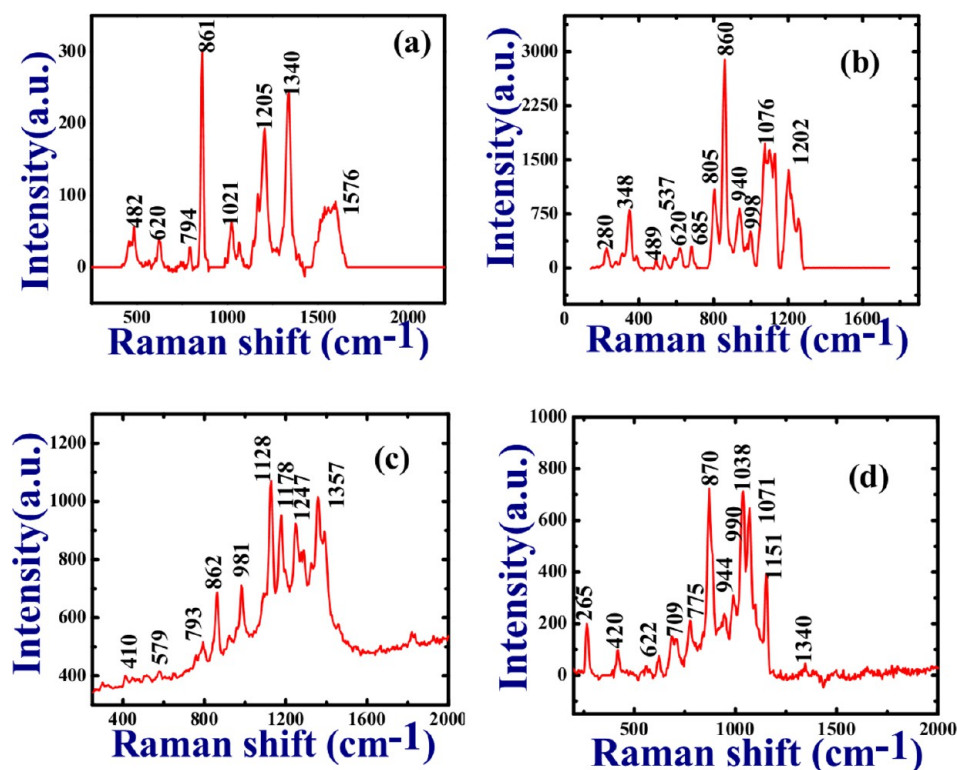


Figure 9. SERS spectra of FOX-7 ($5 \mu\text{M}$ dissolved in acetone) adsorbed on (a) Ag, (b) $\text{Ag}_{0.65}\text{Au}_{0.35}$, (c) $\text{Ag}_{0.5}\text{Au}_{0.5}$, and (d) $\text{Ag}_{0.35}\text{Au}_{0.65}$ nanostructured substrates obtained using femtosecond laser ablation. The time of integration was ~ 0.5 s.

Table 2. Observed Active Raman Modes of FOX-7 Adsorbed on Ag–Au Nanostructures Fabricated by fs Ablation in Acetone^a

S. No.	reported Raman shifts of FOX-7 (in cm^{-1})	assignments	observed Raman shifts from FOX-7 powder (in cm^{-1})	observed surface enhanced Raman shifts from bimetallic nanomaterials (in cm^{-1})
1.	318	out of layer H wagging	318	348
2.	447	in layer sym. NH wagging	455	410, 420
3.	481	sym. NO and NH wagging	477	482, 489
4.	622	out of layer sym. NH wagging	620	620, 622
5.	789	C–NO ₂ rocking	790	775, 794, 795, 805
6.	856	NO and NH rocking	856	860, 861, 862, 870
7.	1024	in layer asym. NH wagging	1024	1021, 1038
8.	1070	in layer sym. NH wagging	1063	1071, 1076
9.	1208	asym. C–NO ₂ stretch + NH wagging	1206	1202, 1247
10.	1343	sym. C–NO ₂ stretch + NH wagging	1346	1340, 1357
11.	1464	C–C stretch + NH wagging	1461	
12.	1528	C–NH ₂ bend + C–C stretch	1524	

^aThe time of integration was 0.5 s for all measurements.

signatures of FOX-7 from Ag–Au NSs were evaluated by considering the adsorption factor to be ~ 0.4 (percentage of FOX-7 molecules adsorbed on the NSs) following the procedure reported in our earlier works.¹⁰ Similar to the case of Au film of NPs, Au NSs demonstrated good elevation of the Raman signatures whose shift is greater than 1145 cm^{-1} and other modes were not elevated much (as shown in Figure 5a of the Supporting Information). The above-mentioned enhancement factors were estimated by comparing the SERS spectra with normal Raman spectra of FOX-7 (0.1 M) on a glass slide (shown in Figure 5b of the Supporting Information). The observed modes of FOX-7 and their detailed assignments⁵¹ are presented in Table 2.

In the above-mentioned two cases of (a) detection of INPZ and (b) detection of FOX-7, the combination of $\text{Ag}_{0.65}\text{Au}_{0.35}$ was observed to demonstrate superior Raman enhancements compared to other combinations and pure Ag and Au nanomaterials. The tunability of LSP resonances plays a crucial role in the optical properties of the materials. Probably the hybridization of metals at these proportions was superior compared to other combinations. Consequently, elevation of Raman signatures was observed due to the enhanced local fields provided by $\text{Ag}_{0.65}\text{Au}_{0.35}$ nanomaterials compared to other combinations. Our observations demonstrated that obvious SERS enhancement was observed when the analyte molecules adsorbed on the Ag–Au system of appropriate proportions.

The combination of Ag–Au metals provides chemical stability to the nanomaterials which could have enhanced the efficacy of SERS activity. When the analyte molecules adsorbed in between the dimers of Ag–Au combination, local electric fields enhance gigantically as a function of separation. Zheng et al.⁵² reported that the increment of Au percentage in Ag–Au core–shell NPs diminishes the SERS activity. One more possible reason could be the dimensionality (smaller dimensions compared to others) of the fabricated NPs/NSs at the proportion used in Ag_{0.65}Au_{0.35}. Fan et al.⁵³ recently demonstrated that SERS enhancements not only depend on the Ag:Au ratio but also on the chemical nature of the analyte molecule. In their studies, they obtained higher Raman signature enhancements from alloy (Ag–Au) NPs with higher gold proportion for the positively charged probes of oxazine 720 (Oxa) and Nile Blue A (NBA). On the other hand, Ag–Au NPs with a higher Ag proportion exhibited superior SERS enhancements for the molecular probes 4-hydroxythiophenol (HTP) and thiophenol (TP) which are negatively charged. This was explained through their DFT calculations which concluded that the charge transfer between Au and Ag atoms in alloy NPs provoke positively charged regions in Ag atoms, whereas negatively charged regions prevail in Au atoms. Thus, obtained charges on surfaces of Ag–Au NPs influence the attachment of analyte molecules on top of the nanomaterials and, consequently, the enhancement factors. Many other studies^{54–64} on Ag–Au bimetallic systems were mainly confined to NPs and their related studies, but in the present study, we have investigated the SERS activity of both bimetallic NPs in acetone (colloidal solutions) as well as NSs (fs laser modified Ag solid targets).

The data (Raman measurements) presented here were an average of several measurements (depending on the integration time). In the case of NPs in film form (drop casted), the Raman intensity at different points could be slightly different (depending on the way the drop is placed on the glass slide). By increasing the number of averages (integration time), we tried to minimize the fluctuations. For practical applications, one requires consistent spectra over a large area of the substrate achieved in the shortest period of time. We anticipate that screen printing⁶⁵ of these NPs could be one possible solution for producing highly reproducible measurements. However, in the case of nanostructures, we achieved reproducibility over a large area, since the nanostructures remained intact after each measurement. We had earlier demonstrated the recycling capability of Cu nanostructures prepared using the same technique.¹⁰ Possible improvements in the present works include (a) grafting of Ag–Au NPs on a germanium/silicon substrate for extra uniform SERS substrates which is a two-step process further enhancing the SERS sensitivity, as documented earlier by Wang et al.;⁶⁶ (b) grafting of Ag–Au NPs on plain gold or silver substrates which incorporates the generation of hot spots those determined by the nanogap between the plain Ag/Au surface and Ag–Au NPs;³⁴ (c) Ag–Au bimetallic NPs can be utilized as SERS sensors on paper through the screen printing technique which facilitates the fabrication of movable SERS sensors and those are directly usable for onsite detection of molecular probes;⁶⁵ (d) Ag–Au NPs with smaller dimensions can be encapsulated with silicon quantum dots in polymeric NPs, enhancing the capability of luminescence and the SERS activity of molecular probes significantly.⁶⁷ The combination of NPs and NSs (by placing NPs on the nanostructured surface as reported by Jin et al.⁶⁸) is another

possibility of improving the detection limits. NPs in the nanogaps of NSs generate an enormous number of hot spots due to the combined plasmonic resonances enhancing the local fields which elevate the Raman signatures of adsorbed analyte molecules. Our future studies will also focus on the photonic applications of such NPs.^{69,70}

CONCLUSIONS

Ag–Au bimetallic targets at different proportions were made by mixing the required proportions of metals followed by melting and cooling the mixture. Thus, prepared mixtures were utilized to make small target strips ($10 \times 10 \text{ mm}^2$) to carry out ablation. Later, these targets were ablated with ~ 40 fs laser pulses in acetone and thus Ag–Au bimetallic nanomaterials (NPs and NSs) were fabricated in a single experiment. Post fabrication Ag–Au NPs and NSs were utilized to detect explosive molecules of FOX-7 and 1NPZ. Our SERS measurements demonstrated enhancement factors in the range 10^6 – 10^8 . This study demonstrated that a specific proportion, Ag_{0.65}Au_{0.35}, is responsible for obtaining very significant SERS enhancements (compared to other proportions) compatible with the explosive probe molecules FOX-7 and 1NPZ. This enhancement is tentatively attributed to the formation of positively charged regions in Ag rich NPs, resulting in significant binding of analyte molecules to the surface of Ag–Au NPs and NSs.

ASSOCIATED CONTENT

Supporting Information

(a) UV–visible absorption spectra of “as prepared colloids”. (b) Raman spectra of nitroprazole powder, on AuNP film, and on a glass slide. (c) High resolution FESEM images of the nanostructured targets. (d) Raman spectra of the FOX-7 molecule on the Au target and a glass slide. The Supporting Information is available free of charge on the ACS Publications website at DOI: 10.1021/acs.jpcc.5b03958.

AUTHOR INFORMATION

Corresponding Author

*E-mail: soma_venu@uohyd.ac.in or soma_venu@yahoo.com. Phone: +91-040-23138811.

Notes

The authors declare no competing financial interest.

ACKNOWLEDGMENTS

The authors acknowledge DRDO, India, for continuous financial support and UPE-II, UoH, for partial financial support.

REFERENCES

- (1) Amendola, V.; Meneghetti, M. Laser Ablation Synthesis in Solution and Size Manipulation of Noble Metal Nanoparticles. *Phys. Chem. Chem. Phys.* **2009**, *11*, 3805–3821.
- (2) Itina, T. E. On Nanoparticles Formation by Laser Ablation in Liquids. *J. Phys. Chem. C* **2011**, *115*, 5044–5048.
- (3) Amendola, V.; Polizzi, S.; Meneghetti, M. Laser Ablation Synthesis of Gold Nanoparticles in Organic Solvents. *J. Phys. Chem. B* **2006**, *110*, 7232–7237.
- (4) Amendola, V.; Riello, P.; Meneghetti, M. Magnetic Nanoparticles of Iron Carbide, Iron Oxide, Iron@Iron Oxide, and Metal Iron Synthesized by Laser Ablation in Organic Solvents. *J. Phys. Chem. C* **2011**, *115*, 5140–5146.
- (5) Podagatlapalli, G. K.; Hamad, S.; Sreedhar, S.; Tewari, S. P.; Venugopal Rao, S. Fabrication and Characterization of Aluminum

Nanostructures and Nanoparticles Obtained Using Femtosecond Ablation Technique. *Chem. Phys. Lett.* **2012**, *530*, 93–97.

(6) Podagatlapalli, G. K.; Hamad, S.; Tewari, S. P.; Sreedhar, S.; Prasad, M. D.; Venugopal Rao, S. Silver Nano-entities Through Ultrafast Double Ablation in Aqueous media for Surface Enhanced Raman Scattering and Photonics Applications. *J. Appl. Phys.* **2013**, *113*, 073106.

(7) Podagatlapalli, G. K.; Hamad, S.; Mohiddon, M. A.; Venugopal Rao, S. Effect of Oblique incidence on Silver Nanomaterials Fabricated in Water via Ultrafast Laser Ablation for Photonics and Explosives Detection. *Appl. Surf. Sci.* **2014**, *303*, 217–232.

(8) Podagatlapalli, G. K.; Hamad, S.; Mohiddon, M. A.; Venugopal Rao, S. Fabrication of Nanoparticles and Nanostructures using Ultrafast Laser Ablation of Silver with Bessel Beams. *Laser Phys. Lett.* **2015**, *12*, 036003.

(9) Hamad, S.; Podagatlapalli, G. K.; Vendamani, V. S.; Nageswara Rao, S. V. S.; Pathak, A. P.; Venugopal Rao, S. Femtosecond Ablation of Silicon in Acetone: Tunable Photoluminescence from Generated Nanoparticles and Fabrication of Surface Nanostructures. *J. Phys. Chem. C* **2014**, *118*, 7139–7151.

(10) Hamad, S.; Podagatlapalli, G. K.; Mohiddon, M. A.; Venugopal Rao, S. Cost Effective Nanostructured Copper Substrates Prepared with Ultrafast Laser Pulses for Explosives Detection using Surface Enhanced Raman Scattering. *Appl. Phys. Lett.* **2014**, *104*, 263104.

(11) Venugopal Rao, S.; Podagatlapalli, G. K.; Hamad, S. Ultrafast Laser Ablation in Liquids for Nanomaterials and Applications. *J. Nanosci. Nanotechnol.* **2014**, *14*, 1364–1388.

(12) Barcikowski, S.; Mafune, F. Trends and Current Topics in the Field of Laser Ablation and Nanoparticle Generation in Liquids. *J. Phys. Chem. C* **2011**, *115*, 4985.

(13) Dallaire, A.-M.; Rioux, D.; Rachkov, A.; Patskovsky, S.; Meunier, M. Laser-Generated Au-Ag Nanoparticles for Plasmonic Nucleic Acid Sensing. *J. Phys. Chem. C* **2012**, *116*, 11370–11377.

(14) Sajti, C. L.; Sattari, R.; Chichkov, B. N.; Barcikowski, S. Gram Scale Synthesis of Pure Ceramic Nanoparticles by Laser Ablation in Liquid. *J. Phys. Chem. C* **2010**, *114*, 2421–2427.

(15) Rehbock, C.; Jakobi, J.; Gamrad, L.; van der Meer, S.; Tiedemann, D.; Taylor, U.; Kues, W.; Rath, D.; Barcikowski, S. Current State of Laser Synthesis of Metal and Alloy Nanoparticles as Ligand-free Reference Materials for Nano-toxicological Assays. *Beilstein J. Nanotechnol.* **2014**, *5*, 1523–1541.

(16) Hajiesmaeilbaigi, F.; Motamedi, A. Synthesis of Au/Ag Alloy Nanoparticles by Nd:YAG Laser Irradiation. *Laser Phys. Lett.* **2007**, *4*, 133–137.

(17) Toshima, N.; Yonezawa, T. Bimetallic Nanoparticles—Novel Materials for Chemical and Physical Applications. *New J. Chem.* **1998**, *22*, 1179–1201.

(18) Compagnini, G.; Messina, E.; Puglisi, O.; Cataliotti, R. S.; Nicolosi, V. Spectroscopic Evidence of a Core–Shell Structure in the Earlier Formation Stages of Au–Ag Nanoparticles by Pulsed Laser Ablation in Water. *Chem. Phys. Lett.* **2008**, *457*, 386–390.

(19) Wang, A. Q.; Liu, J. H.; Lin, S. D.; Lin, T. S.; Mou, C. Y. A Novel Efficient Au–Ag Alloy Catalyst System: Preparation, Activity, and Characterization. *J. Catal.* **2005**, *233*, 186–197.

(20) Wang, A. Q.; Chang, C. M.; Mou, C. Y. Evolution of Catalytic Activity of Au–Ag Bimetallic Nanoparticles on Mesoporous Support for CO Oxidation. *J. Phys. Chem. B* **2005**, *109*, 18860–18867.

(21) Intartaglia, R.; Das, G.; Bagga, K.; Gopalakrishnan, A.; Genovese, A.; Povia, M.; Di Fabrizio, E.; Cingolani, R.; Diaspro, A.; Brandi, F. Laser Synthesis of Ligand Free Bimetallic Nanoparticles for Plasmonic Applications. *Phys. Chem. Chem. Phys.* **2013**, *15*, 3075–3082.

(22) Kuladeep, R.; Jyothi, L.; Ali, S. S.; Deepak, K. L. N.; Narayana Rao, D. Laser-assisted Synthesis of Au-Ag Alloy Nanoparticles with Tunable Surface Plasmon Resonance Frequency. *Opt. Mater. Express* **2012**, *2*, 161–172.

(23) Shah, A.; Rahman, L.-U.; Qureshi, R.; Rehman, Z.-U. Synthesis, Characterization and Applications of Bimetallic (Au-Ag, Au-Pt, Au-Ru) Alloy Nanoparticles. *Rev. Adv. Mater. Sci.* **2012**, *30*, 133–149.

(24) Bansal, A.; Sekhon, J. S.; Verma, S. S. Scattering Efficiency of LSPR Tunability of Bimetallic Ag, Au, and Cu Nanoparticles. *Plasmonics* **2014**, *9*, 143–150.

(25) Adamovic, N.; Schmid, U. Potential of Plasmonics in Photovoltaic Solar Cells. *Elektrotech. Inftech.* **2011**, *128*, 342–347.

(26) Tan, K. S.; Cheong, K. Y. Advances of Ag, Cu, and Ag-Cu alloy Nanoparticles Synthesized via Chemical Reduction Route. *J. Nanopart. Res.* **2013**, *15*, 1537.

(27) Lu, L.; Burkey, G.; Halaciuga, I.; Goia, D. V. Core-shell Gold/Silver Nanoparticles: Synthesis and Optical Properties. *J. Colloid Interface Sci.* **2013**, *392*, 90–95.

(28) Beyene, H. T.; Chakravadhanula, V. S. K.; Hanisch, C.; Strunskus, T.; Zaporozhtchenko, V.; Elbahri, M.; Faupel, F. Vapor Phase Deposition, Structure, and Plasmonic Properties of Polymer-based Composites Containing Ag-Cu Bimetallic Nanoparticles. *Plasmonics* **2012**, *7*, 107–114.

(29) Shin, K. S.; Kim, J. H.; Kim, I. H.; Kim, K. Novel Fabrication and Catalytic Applications of Poly(ethyleneimine)-Stabilized Gold-Silver Alloy Nanoparticles. *J. Nanopart. Res.* **2012**, *14*, 735.

(30) Liu, S.; Chen, G.; Prasad, P. N.; Swihart, M. T. Synthesis of Monodisperse Au, Ag, and Au-Ag Alloy Nanoparticles with Tunable Size and Surface Plasmon Resonance Frequency. *Chem. Mater.* **2011**, *23*, 4098–4101.

(31) Hodak, J. H.; Henglein, A.; Giersig, M.; Hartland, G. V. Laser Induced Diffusion in Au-Ag Core Shell Nanoparticles. *J. Phys. Chem. B* **2000**, *104*, 11708–11718.

(32) Chen, Y.-H.; Yeh, C.-S. A New Approach for the Formation of Alloy Nanoparticles: Laser Synthesis of Gold-Silver Alloy from Gold-Silver Colloidal Mixtures. *Chem. Commun.* **2001**, *4*, 371–372.

(33) Liusman, C.; Li, H.; Lu, G.; Wu, J.; Boey, F.; Li, S.; Zhang, H. Surface-Enhanced Raman Scattering of Ag-Au Nano-disk Heterodimers. *J. Phys. Chem. C* **2012**, *116*, 10390–10395.

(34) Kim, K.; Choi, J.; Shin, K. S. Enhanced Raman Scattering in Gaps Formed by Planar Au and Au/Ag Alloy Nanoparticles. *J. Phys. Chem. C* **2013**, *117*, 11421–11427.

(35) Kim, K.; Kim, K. L.; Choi, J.; Lee, H. B.; Shin, K. S. Surface Enrichment of Ag Atoms in Au/Ag Alloy Nanoparticles Revealed by Surface-Enhanced Raman Scattering of 2,6-Dimethylphenyl Isocyanide. *J. Phys. Chem. C* **2010**, *114*, 3448–3453.

(36) Nedderson, J.; Chumanov, G.; Cotton, T. M. Laser Ablation of Metals: A New Method for Preparing SERS Active Colloids. *Appl. Spectrosc.* **1993**, *47*, 1959–1964.

(37) Prochazka, M.; Stephanek, J.; Vico, B.; Stephanek, J.; Turpin, P. Y. Probing Applications of Laser-Ablated Ag Colloids in SERS Spectroscopy: Improvement of Ablation Procedure and SERS Spectral Testing. *Anal. Chem.* **1997**, *69*, 5103–5108.

(38) Menéndez-Manjón, A.; Wagnen, P.; Barcikowski, S. Transfer-matrix Method for Efficient Ablation by Pulsed Laser Ablation and Nanoparticle Generation in Liquids. *J. Phys. Chem. C* **2011**, *115*, 5108–5114.

(39) Chen, D. H.; Chen, C. J. Formation and Characterization of Au–Ag Bimetallic Nanoparticles in Water-in-oil Micro-emulsions. *J. Mater. Chem.* **2002**, *12*, 1557–1562.

(40) Lee, I.; Han, S. W.; Kim, K. Production of Au–Ag alloy Nanoparticles by Laser Ablation of Bulk Alloys. *Chem. Commun.* **2001**, *18*, 1782–1783.

(41) Han, S. W.; Kim, Y.; Kim, K. Dodecanethiol-Derivatized Au/Ag Bimetallic Nanoparticles: TEM, UV/VIS, XPS, and FTIR Analysis. *J. Colloid Interface Sci.* **1998**, *208*, 272–278.

(42) Papavassiliou, G. C. Surface plasmons in Small Au-Ag alloy Particles. *J. Phys. F: Met. Phys.* **1976**, *6*, L103.

(43) Teo, B. K.; Keating, K.; Kao, Y.-H. Observation of Plasmon Frequency in the Optical Spectrum of Au₁₈Ag₂ Cluster: The Beginning of the Collective Phenomenon Characteristic of the Bulk? *J. Am. Chem. Soc.* **1987**, *109*, 3494.

(44) Sinzig, J.; Radtke, U.; Quinten, M.; Kreibitz, U. Binary clusters: Homogeneous Alloys and Nucleus-shell Structures. *Z. Phys. D: At., Mol. Clusters* **1993**, *26*, 242–245.

- (45) Link, S.; Wang, Z. L.; El-Sayed, M. A. Alloy Formation of Gold–Silver Nanoparticles and the Dependence of the Plasmon Absorption on Their Composition. *J. Phys. Chem. B* **1999**, *103*, 3529–3533.
- (46) Olea-Mejía, O.; Fernández-Mondragón, M.; Rodríguez-de la Concha, G.; Camacho-López, M. SERS-Active Ag, Au and Ag–Au Alloy Nanoparticles Obtained by Laser Ablation in Liquids for Sensing Methylene Blue. *Appl. Surf. Sci.* **2015**, *348*, 66–70.
- (47) LeBlanc, M.; Erler, W. Röntgenographische Untersuchungen des Mischkristallsystems Gold-Silber und Umtersuchungsmittel seine Artgreifbarkeit durch Salpetersäure. *Ann. Phys.* **1933**, *408*, 321.
- (48) Catchpole, K. R.; Polman, A. Plasmonic Solar Cells. *Opt. Express* **2008**, *16*, 21793–21800.
- (49) Le Ru, E. C.; Etchegoin, P. G. Phenomenological Local Field Enhancement Factor Distributions Around Electromagnetic Hot Spots. *J. Chem. Phys.* **2009**, *130*, 181101–4.
- (50) Nageswara Rao, E.; Ravi, P.; Tewari, S. P.; Venugopal Rao, S. Experimental and Theoretical Studies on the Structure and Vibrational Properties of Nitropropanes. *J. Mol. Struct.* **2013**, *1043*, 121–131.
- (51) Dreger, Z. A.; Tao, Y.; Gupta, Y. M. High-Pressure Vibrational and Polymorphic Response of 1,1-Diamino-2,2-dinitroethene Single Crystals: Raman Spectroscopy. *J. Phys. Chem. A* **2014**, *118*, 5002–5012.
- (52) Zheng, Z.; Shan, G.; Li, J.; Chen, Y.; Liu, Y. Au/Ag Nano Alloy Shells as Near Infrared SERS Nano-probe for the Detection of Protein. *Mater. Res. Express* **2014**, *1*, 045408.
- (53) Fan, M.; Lai, F.; Chou, H.; Lu, W.; Hwang, B.; Brolo, A. G. Surface-enhanced Raman Scattering (SERS) from Au:Ag Bimetallic Nanoparticles: The Effect of the Molecular Probe. *Chem. Sci.* **2013**, *4*, 509–515.
- (54) Kim, K.; Choi, J.; Shin, K. S. Raman Scattering Characterization of 1,4-phenylenediamine in Au–Au and Ag–Au Nanogaps. *Spectrochim. Acta, Part A* **2013**, *100*, 3–9.
- (55) Kim, K.; Kim, K. L.; Lee, S. J. Surface Enrichment of Ag atoms in Au/Ag alloy Nanoparticles Revealed by Surface Enhanced Raman Scattering Spectroscopy. *Chem. Phys. Lett.* **2005**, *403*, 77–82.
- (56) Liao, X.; Chen, Y.; Qin, M.; Chen, Y.; Yang, L.; Zhang, H.; Tian, Y. Au–Ag–Au Double Shell Nanoparticles-based Localized Surface Plasmon Resonance and Surface-enhanced Raman Scattering Biosensor for Sensitive Detection of 2-mercapto-1-methylimidazole. *Talanta* **2013**, *117*, 203–208.
- (57) Gellner, M.; Küstner, B.; Schlucker, S. Optical Properties and SERS Efficiency of Tunable Gold/Silver Nanoshells. *Vib. Spectrosc.* **2009**, *50*, 43–47.
- (58) Wu, P.; Gao, Y.; Zhang, H.; Cai, C. Aptamer-Guided Silver-Gold Bimetallic Nanostructures with Highly Active Surface-Enhanced Raman Scattering for Specific Detection and Near-Infrared Photothermal Therapy of Human Breast Cancer Cells. *Anal. Chem.* **2012**, *84*, 7692–7699.
- (59) Bu, Y.; Lee, S. Influence of Dopamine Concentration and Surface Coverage of Au Shell on the Optical Properties of Au, Ag, and Ag Nanoparticles. *ACS Appl. Mater. Interfaces* **2012**, *4*, 3923–3931.
- (60) Bai, T.; Sun, J.; Che, R.; Xu, L.; Yin, C.; Guo, Z.; Gu, N. Controllable Preparation of Core-Shell Au-Ag Nanoshuttles with Improved Refractive Index Sensitivity and SERS Activity. *ACS Appl. Mater. Interfaces* **2014**, *6*, 3331–3140.
- (61) Yang, Y.; Zhang, Q.; Fu, Z. W.; Qin, D. Transformation of Ag Nanocubes into Ag-Au Hollow Nanostructures with Enriched Ag Contents to Improve SERS Activity and Chemical Stability. *ACS Appl. Mater. Interfaces* **2014**, *6*, 3750–3757.
- (62) Mulvaney, P. Surface Plasmon Spectroscopy of Nano Sized Metal Particles. *Langmuir* **1996**, *12*, 788–800.
- (63) Sebastian, S.; Linsal, C. L.; Vallbhan, C. P. G.; Nampoore, V. P. N.; Radhakrishnan, P.; Kailasnath, M. Formation of Au-Ag Nanoalloy Through Au core/Ag Shell Intermediate Phase by Laser Ablation. *Chem. Phys. Lett.* **2015**, *628*, 25–29.
- (64) Wang, T.; Hu, F.; Ikhile, E.; Liao, F.; Li, Y.; Shao, M. Two-step-route to Ag–Au Nanoparticles Grafted on Ge Wafer for Extra-uniform SERS Substrates. *J. Mater. Chem. C* **2015**, *3*, 559–563.
- (65) Ou, Y.; Wang, L.; Zhu, L.; Wan, L.; Xu, Z. In-Situ Immobilization of Silver Nanoparticles on Self-Assembled Honeycomb-patterned Films Enables Surface-Enhanced Raman Scattering (SERS) Substrates. *J. Phys. Chem. C* **2014**, *118*, 11478–11484.
- (66) Qu, L.-L.; Song, Q.; Li, Y.; Peng, M.; Li, D.; Chen, L.; Fossey, J. S.; Long, Y. Fabrication of Bimetallic Microfluidic Surface-Enhanced Raman Scattering Sensors on Paper by Screen Printing. *Anal. Chim. Acta* **2013**, *792*, 86–92.
- (67) Harun, N. A.; Horrocks, B. R.; Fulton, D. A. Enhanced Raman and Luminescence Spectra from Co-encapsulated Silicon Quantum Dots and Ag-Au Nano alloys. *Chem. Commun.* **2014**, *50*, 12389–12391.
- (68) Jin, Z.; Gu, W.; Shi, X.; Wang, Z.; Jiang, Z.; Liao, L. A Novel Route to Surface-Enhanced Raman Scattering: Ag Nanoparticles Embedded in the Nano-gaps of a Ag Substrate. *Adv. Opt. Mater.* **2014**, *2*, 588–596.
- (69) Hamad, S.; Podagatlapalli, G. K.; Tewari, S. P.; Venugopal Rao, S. Influence of Picosecond Multiple/single Line Ablation on Copper Nanoparticles Fabricated for Surface Enhanced Raman Spectroscopy and Photonics Applications. *J. Phys. D: Appl. Phys.* **2013**, *46*, 485501.
- (70) Papagiannouli, I.; Aloukos, P.; Rioux, D.; Meunier, M.; Couris, S. Effect of the Composition on the Nonlinear Optical Response of Au_xAg_{1-x} Nano-Alloys. *J. Phys. Chem. C* **2015**, *119*, 6861–6872.